JOURNAL OF SPACECRAFT AND ROCKETS
Vol. 44, No. 5, September–October 2007

System Approach to Performance Verification of the Planck Cryogenic Spacecraft

Ravinder S. Bhatia,* Claudio Damasio,† and Bernard Guillaume‡
ESA, 2200 AG Noordwijk, The Netherlands

DOI: 10.2514/1.24036

The scientific objectives of the Planck mission include observations of the temperature anisotropy of the cosmic microwave background. With a target launch date of early 2008, Planck will be inserted into the Lagrange-2 point of the Earth–sun system. The payload comprises two instruments with focal planes operating at 20 and 0.1 K, respectively. We describe the verification of the design of the Planck cryogenic chain, which consists of five stages of cooling. The first stage uses multiple V-groove and high-emissivity radiators to passively reach a temperature of less than 60 K. The second stage of cooling uses thermal compression and Joule–Thomson expansion of hydrogen in a sorption cooler that achieves a temperature of 20 K for operation of the Low Frequency Instrument and a temperature of 18 K for precooling of the High Frequency Instrument. The third stage of cooling uses Joule–Thomson expansion of helium-4 to achieve a temperature of 4.5 K for cooling of the Low Frequency Instrument radiometer reference loads and for further precooling of the High Frequency Instrument. The final cooler uses dilution of helium-4 and helium-3 isotopes to achieve a base temperature of 0.1 K for operation of the High Frequency Instrument detectors, with the dilution return mixture expanded through a Joule–Thomson orifice to provide additional cooling at 1.6 K. The complex interfaces between instruments and coolers on Planck result in highly interdependent thermal performance between the subsystems. To verify the system-level performance of the complete cooling chain, a system-level thermal model was built that incorporates the subsystem thermal models of the complete cooling chain and the payload instruments and that predicts the cooldown and steady-state performance of the Planck flight model. These modeling predictions demonstrate by analysis that the flight model thermal design meets the requirements for in-orbit performance. To complement these analyses, additional performance verification by test was performed through on-ground testing of the Planck cryogenic qualification model. In this test, the required cooldown performance and final base temperatures were achieved, including the 0.1 K temperature needed for the coldest detectors. To guide the definition and execution of the test, the system thermal model was adapted to reflect the precise configuration of the tested hardware and to include the thermal shrouds and baffles of the cryogenic test facility. The predictions of this modified thermal model are presented as a preliminary correlation against actual test data. Good agreement was obtained between the experimental data and the model predictions, and we conclude that a high degree of confidence in the performance of the Planck cooling chain was gained at the system level.

Nomenclature

E_{01}	=	efficiency factor for the sorption cooler heat exchanger
H	=	enthalpy of the working fluid
M	=	mass flow rate
P_{HIGH}	=	pressure of the high-pressure sorption gas
P_{LOW}	=	pressure of the low-pressure sorption gas
Q	=	cooling power
Q_{PC1}	=	heat load from the sorption cooler onto the warmest V-groove radiator
Q_0	=	sum of the thermal dissipation and parasitic heat load
q_{DIL}	=	dilution cooling power assuming simplified thermodynamic properties for the working fluids
T	=	temperature
T_{PC1}	=	temperature of the first sorption precooler (at the warmest V-groove radiator)
T_{SCC}	=	temperature of the hydrogen gas exiting the sorption compressor

Received 31 March 2006; revision received 2 November 2006; accepted for publication 1 December 2006.

*Senior Thermal/Cryogenics Engineer, European Space Research and Technology Center, Thermal and Environmental Control Section, Postbus 299; Ravinder.Bhatia@esa.int. Member AIAA.

†Thermal System Engineer, European Space Research and Technology Center, Thermal and Environmental Control Section, Postbus 299; Claudio.Damasio@esa.int.

‡Payload System Engineer, European Space Research and Technology Center, Herschel/Planck Project, Postbus 299; Bernard.Guillaume@esa.int.

I. Introduction

THE scientific objectives of the Planck mission include mapping of the cosmic microwave background (CMB) anisotropies, measurement of the amplitude of CMB structures, determination of the Hubble constant, and testing of inflationary models of the early universe. Planck will be launched by an Ariane 5 vehicle, together with the Herschel Space Observatory, to a Lissajous orbit about the L2 Lagrange point of the Earth–sun system, with a target launch date of 2008 [1]. The spacecraft will spin at one revolution per minute and perform two full-sky surveys of the CMB during a lifetime of 18 months, over a range of observational wavelengths.

The science objectives require the sensitivity to detect temperature fluctuations on the order of better than one part in 10^5 of the nominal 2.7 K temperature of the CMB. To meet this challenging requirement, the detectors must operate at temperatures sufficiently low to allow the required levels of sensitivity and speed of response to be achieved. The detectors for the Low Frequency Instrument (LFI) and the High Frequency Instrument (HFI) operate at temperatures of 20 and 0.1 K, respectively. In addition, the instrument optics and surroundings must also be cryogenically cooled to reduce radiative emission onto the detector focal planes. Rather than using a cryostat with expendable cryogens for cooling, which could potentially impose constraints on the mission lifetime, payload mass, and mission cost, Planck uses a complex chain of cryocoolers linked in series to achieve successively colder stages. For many spacecraft, the coolers and instruments are almost

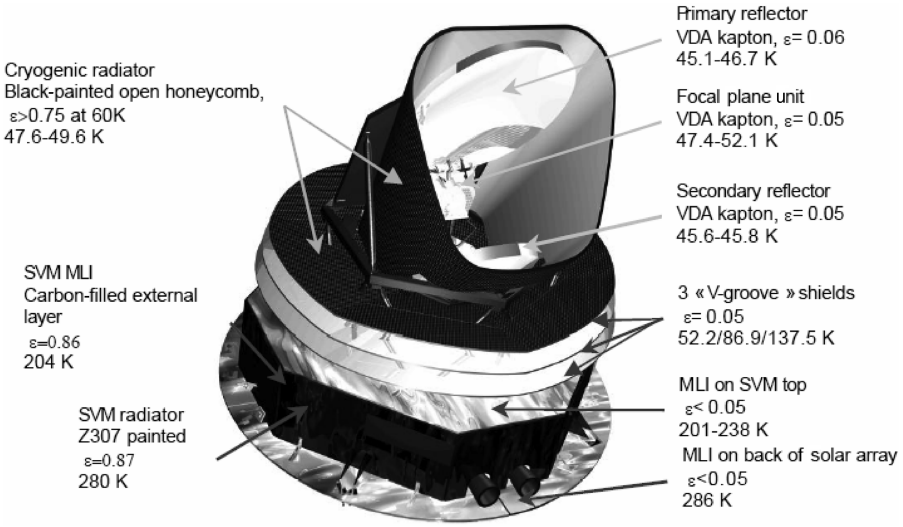

Fig. 1 Planck spacecraft major thermal design features.

standalone black boxes that are bolted onto the structure and that have little thermal interaction with the other subsystems of the spacecraft. This design philosophy is reflected, for example, in the Envisat spacecraft, with ten payload instruments and two pairs of active coolers [2]. However, the design architecture of Planck is particularly challenging because of the complex thermal interactions between all of its subsystems. To accommodate and link the individual coolers and the payload instruments, the design of Planck must simultaneously address a number of thermal, optical, and mechanical demands [3]. All of this leads to the need to have a modeling tool that can be used to help verify the basic thermal design of the complete spacecraft.

The overall verification approach for the Planck thermal design is performed though a combination of analysis (modeling) and testing. Verification by analysis is performed using the system-level modeling tool, which guides the design of the protoflight model (PFM) and gives confidence in the expected in-orbit performance of Planck. Validation of the system model itself is performed first through correlation with the cryogenic qualification model (CQM) test data. The system thermal model is then refined in preparation for the later PFM tests.

This paper first describes the thermal design of the subsystems of Planck. This is followed by a summary of the thermal modeling of these subsystems, together with a description of the manner in which these individual models were integrated in a system-level thermal model. A summary of the CQM test results will then be presented, along with a preliminary correlation of the model with these test results. Finally, the lessons learned from this program of work and the associated conclusions are presented.

II. Thermal Requirements and Design

The Planck top-level thermal requirements derive from the need for cryogenic cooling of 1) the scientific instruments to achieve required instrument sensitivities and 2) the surroundings of the instruments to reduce thermal self-emission from these components against which the scientific signals would otherwise be lost. The spacecraft will initially be at ambient temperature and will cool down during the cruise phase. The payload will be kept permanently in solar shadow, with the spin axis pointing toward the sun. In this way, the payload will be protected from direct solar illumination by the rest of the spacecraft. Because of the limited cooling power available for refrigeration of the payload module, there is a need to keep the heat load from the service module to the payload module as low as possible. The spacecraft therefore makes use of thermal decoupling between the cryogenic payload module and ambient temperature service module. A schematic of the spacecraft is shown in Fig. 1, highlighting the main thermal design features that will now be described.

A. Spacecraft

1. *Service Module*

The Planck service module (SVM) is an octagonal-shaped box supporting a circular solar array and housing the warm parts of the scientific instruments and the spacecraft control subsystems. The nominal temperature of the SVM must be close to 300 K. The top of the SVM, composed of a circular equipment platform and upper closure panels, is covered by aluminized multilayer insulation (MLI) blankets to minimize the thermal loads on the payload module. For the same reason, the rear side of the external portions of solar arrays is covered by aluminized MLI blankets.

2. *Payload Module*

Exploded and assembled views of the PLM are shown in Figs. 2 and 3, respectively. The Planck payload module (PLM) is composed of the telescope, the telescope baffle to reduce the stray light that would otherwise enter the telescope optics, a series of three radiators, and the cryogenic parts of the two instruments. The PLM is mechanically supported via low-thermal-conductivity struts on the SVM. The requirement on the telescope in-flight temperature is that it must be passively cooled to below 50 K. A characterization program to guide the selection of materials for the PLM has been carried out at cryogenic temperatures [4].

B. Coolers

Here, we describe the passive radiative cooling and three active coolers on Planck. Care was taken with the design of each active cooler to ensure that its thermodynamic performance is not compromised in a zero-gravity environment.

1. *Payload Module Radiative Coolers*

The PLM makes use of V-groove radiators that have the dual function of minimizing the radiative flux coming from the SVM and rejecting this flux to space. The radiators are three canted shields [5,6] made of aluminum honeycomb panels covered with two aluminum skins at high purity (99.99%), thereby maximizing the radiative decoupling. In addition, the shields are inclined with a 5-deg angle between successive shields. This design feature rejects part of the remaining heat flow to deep space through multiple reflections. Each shield has six internal flat segments surrounded by dismountable external segments, with all sections made from aluminum. The telescope baffle and the upper surface of the third V-groove (facing the telescope baffle) are highly emissive, to radiate the remaining heat flow to space. The high effective emissivity of the surfaces is obtained through the use of black-painted open honeycomb. The V-groove temperature requirements are given in

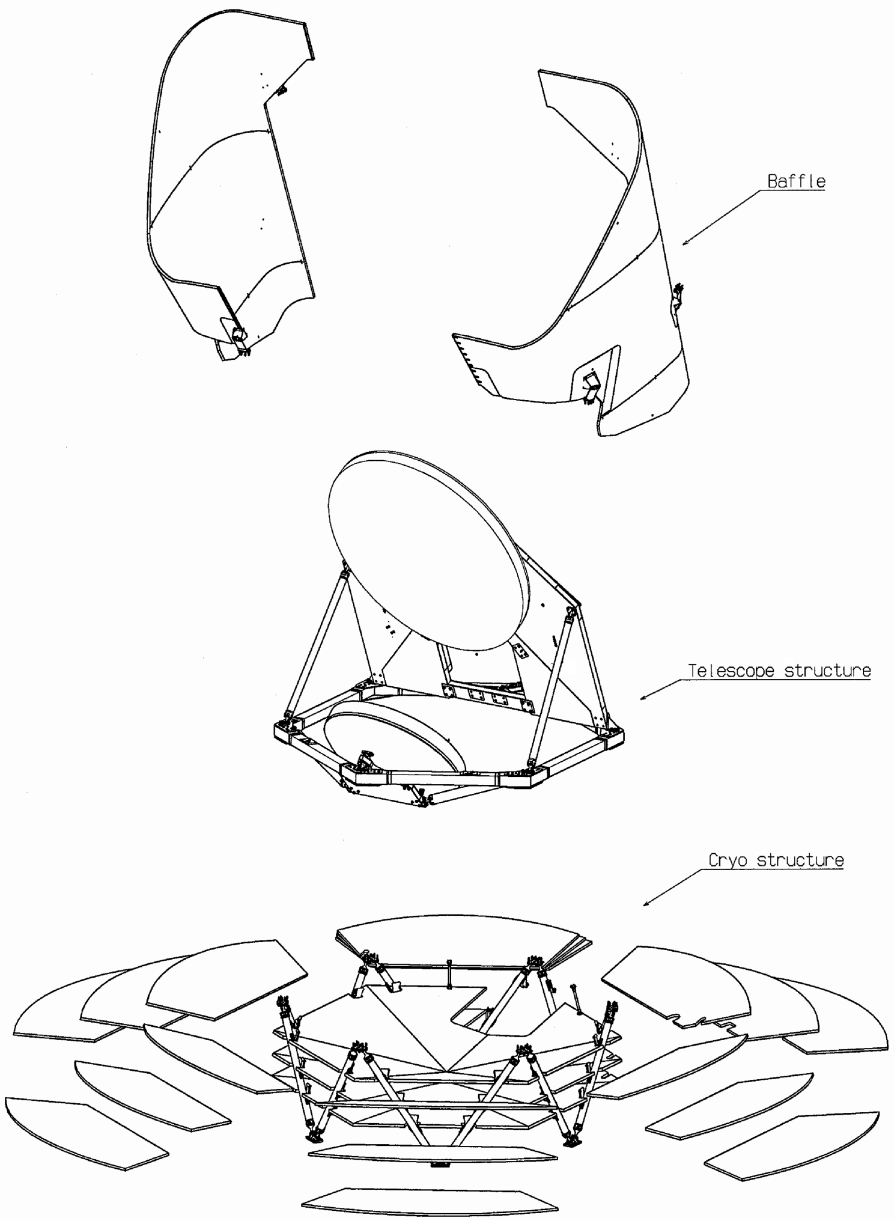

Fig. 2 Planck payload module, exploded view.

Table 1 (note that the payload instrument interfaces have a separate set of thermal requirements).

2. Hydrogen Sorption Cooler

The 20 K sorption cooler uses thermal compression of hydrogen followed by Joule–Thomson (JT) expansion through an orifice to cool both payload instruments [7]. A schematic of the cooler is shown in Fig. 4. To obtain a constant supply of high-pressure refrigerant, a sequence of six hydride beds (Fig. 5) is used to alternately desorb and adsorb the hydrogen gas. Gas-gap heat switches are used to connect or thermally isolate the compressors from a dedicated radiator on the SVM [8]. Hydrogen at 48 bar pressure is precooled to below its JT inversion temperature through thermal contact with the shields of each V-groove radiator, with three thermal interfaces at the third V-groove, to improve heat transfer at this final precooling stage. The hydrogen is then expanded through a JT restrictor [9] into the two-phase region. The liquid evaporates under the heat load from the instruments to be cooled, and the gas returns via recuperative heat exchangers to the compressor sorbent beds. The sorption cooler performance requirement is a cooling power of $\sim$1 W for a cold end temperature of less than 20 K, at a final precooling temperature of 60 K. The heat load allocations for the interfaces of the sorption cooler with the spacecraft are given in Table 2.

3. Helium Joule–Thomson Cooler

A closed-cycle mechanical cryocooler for Planck has been developed at the Rutherford Appleton Laboratory (RAL) to achieve a base temperature of 4 K [10]. Two compressors compress the helium gas to pressures of approximately 1 and 9 bar. The helium passes through three counterflow recuperative heat exchangers and then a JT expansion orifice to achieve cooling. An ancillary panel housed in the spacecraft service module includes a getter and filter to ensure the purity of the gas, thus preventing the JT orifice from becoming blocked with contaminants. A low-vibration electronics unit manages the cooler housekeeping data, getter heating voltage, and cooler drive voltage waveforms. These drive waveforms are under active control to reduce self-induced compressor vibrations up to the fifth harmonic. In addition to generating microphonic pickup on the detector signals, these vibrations also have a dissipative heating effect that could reduce the final cooling power available at the 0.1 K stage. Cold-temperature plumbing includes the heat exchangers, filters, and gas purifiers on each cooling stage. At the 4 K cold end

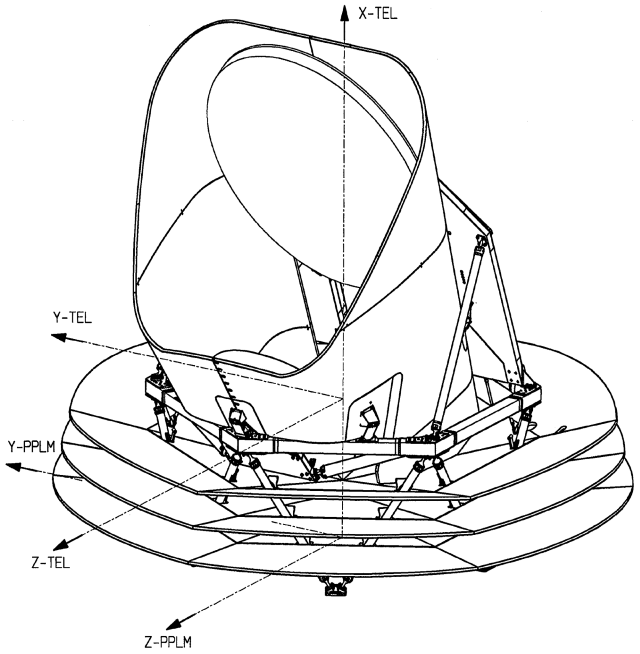

Fig. 3 Planck payload module.

(Fig. 6), a sintered reservoir contains the liquid helium in zero gravity. Figure 7 shows a schematic of the cooler assembly.

4. Helium Dilution Cooler

In a dilution cooler, pure ^{3}He and ^{4}He isotopes are precooled in a heat exchanger, then mixed together to produce cooling due to the enthalpy difference between the pure isotopes and the dilute mixture. Above 0.87 K, a ^{3}He-^{4}He mixture is in a single phase state for all concentrations of ^{3}He, and so separation is never observed. For mixtures below 0.87 K with a concentration of ^{3}He greater than 6.4%, the mixture separates into two phases, one of which is rich in ^{4}He and the other of which is rich in ^{3}He. As the temperature is reduced, the concentration of ^{3}He on the diluted side tends to a constant value of 6.4%, so that even at the lowest temperatures, ^{3}He remains dissolved in superfluid ^{4}He [11].

The dilution system on Planck is designed to meet the difficult challenge of operating without the use of gravity for separation of the ^{3}He and ^{4}He in the still [12]. The system was developed by the Centre de Recherches sur les Très Basses Températures (CRTBT) and is being space-qualified by Air Liquide. As shown in Fig. 8, the

Table 1 Thermal requirements for V-groove radiators

V-groove	Maximum temperature, K
V-groove 1	160
V-groove 2	100
V-groove 3	60

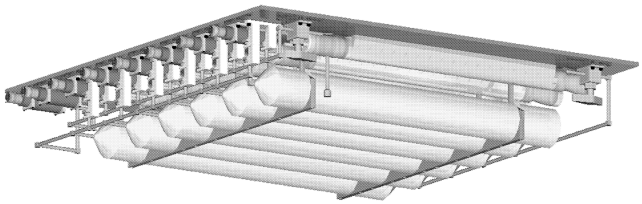

Fig. 5 Compressor assembly for the 20 K sorption cooler (from [20]).

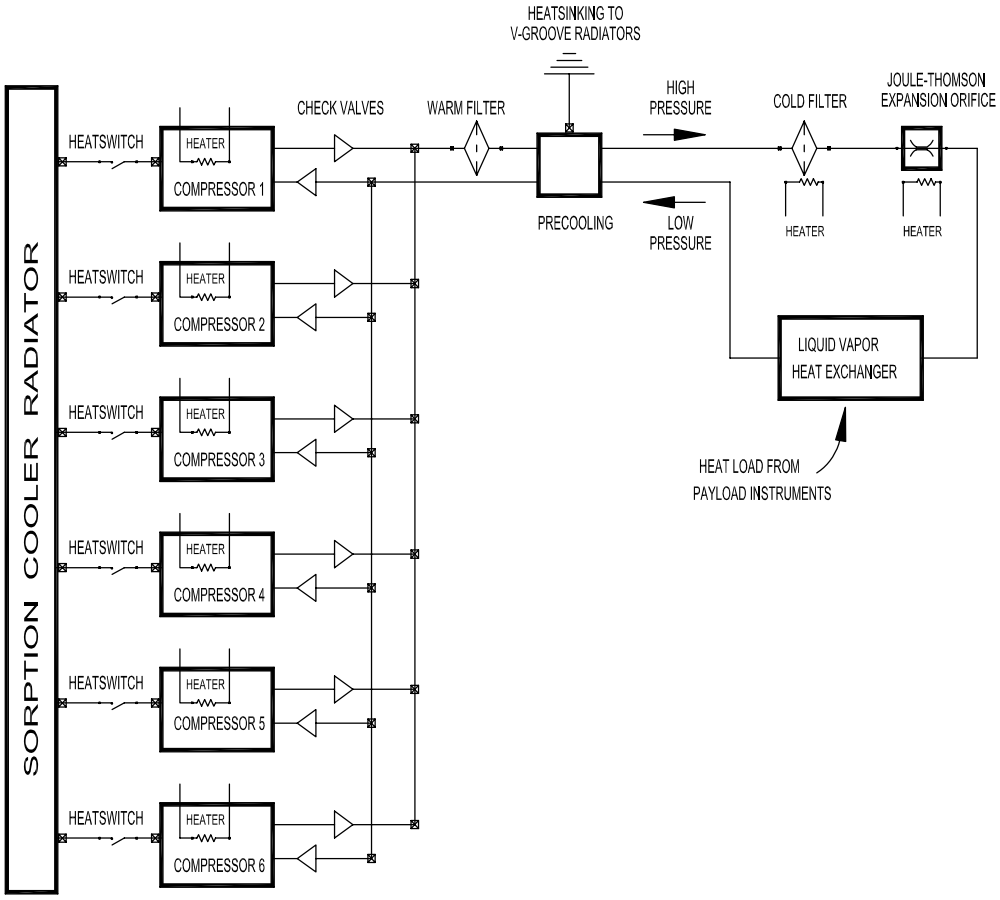

Fig. 4 Schematic of the 20 K sorption cooler.

Table 2 Sorption cooler heat load requirements

Interface	Requirement on maximum temperature, K	Requirement on maximum heat load, mW
V-groove 1	160	566
V-groove 2	100	447
V-groove 3	60	1175

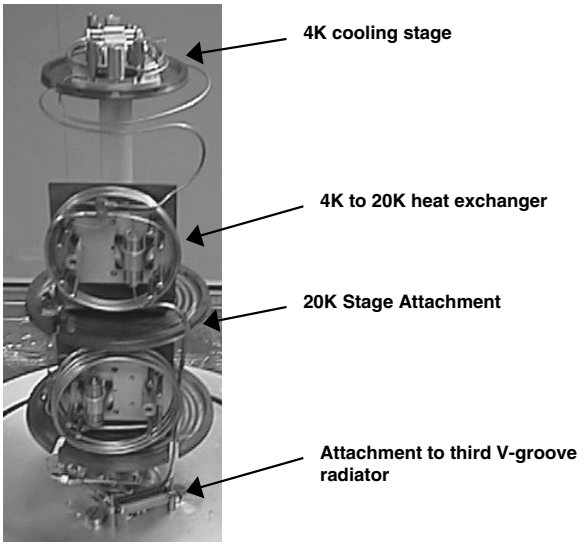

Fig. 6 Photograph of the 4 K cooler cold end.

isotopes flow from the storage tanks through the control unit and the piping via counterflow heat exchangers and charcoal filters to the 0.1 K stage. The cooling performance of the dilution cooler is susceptible to microvibrations, which could be created by the pumping system and/or by the circulation of the cryogenic fluids. The design of Planck at the system level and the test program must therefore ensure that these microvibrations are not introduced at unduly high levels.

C. Payload Instruments

We now give an overview of the design of each of the two payload instruments, focusing on their thermal/cryogenic cooling needs.

1. Low Frequency Instrument

The Low Frequency Instrument is a radiometer receiver array that is designed to produce high-sensitivity multifrequency measurements of the microwave sky in the frequency range of 27 to 77 GHz (wavelength range of 11.1 to 3.9 mm) [13]. The radiometer concept is chosen to maximize the stability of the instrument by reducing the effect of nonwhite noise generated in the radiometer itself. In this scheme, the difference between the inputs to each of the chains (the signal from the telescope and that from a reference black body, respectively) is continuously observed. To remove the effect of instability in the back-end amplifiers and detector diodes, it is necessary to switch the signal detected at the diodes at high rate. To achieve the required level of sensitivity, the LFI uses low-noise amplifiers that require cryogenic cooling down to 20 K. To reduce the heat load to the focal plane, the radiometers are split into two subassemblies connected by waveguides, one located at the PLM, the other on the SVM. These design features allow the power dissipation of the entire front-end low-noise amplifier to be less than

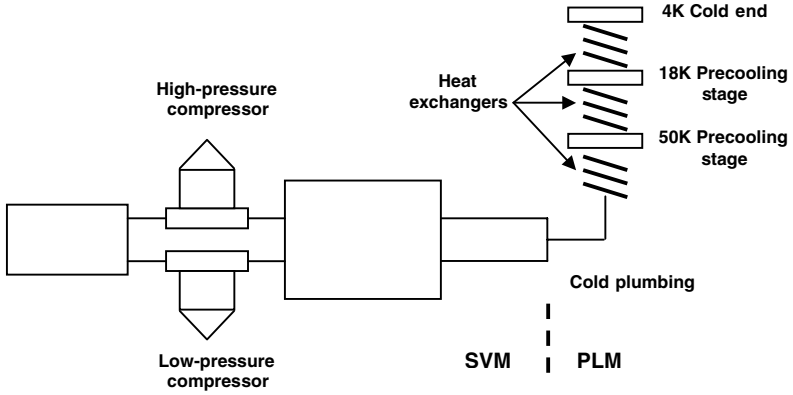

Fig. 7 Schematic of the 4 K cooler.

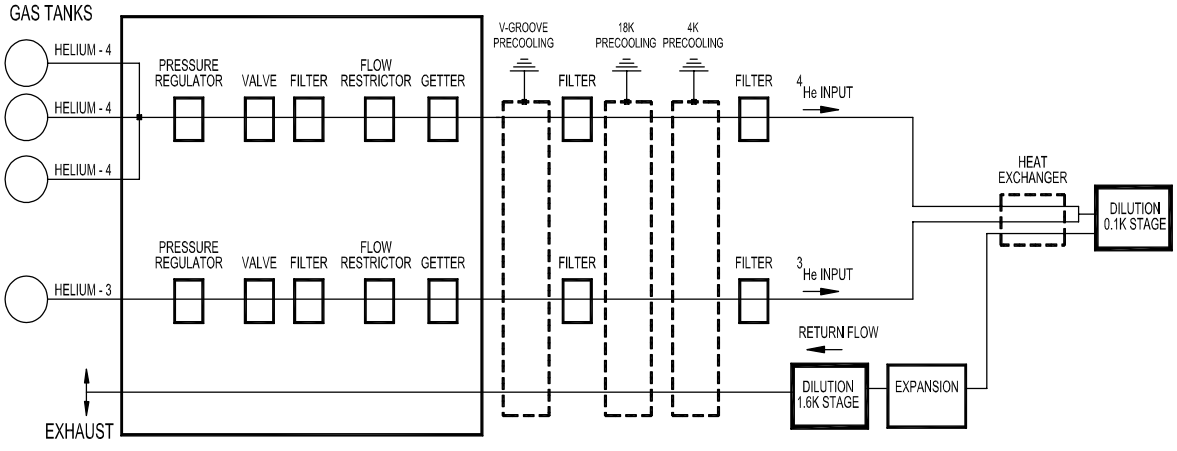

Fig. 8 Simplified schematic of the dilution cooler.

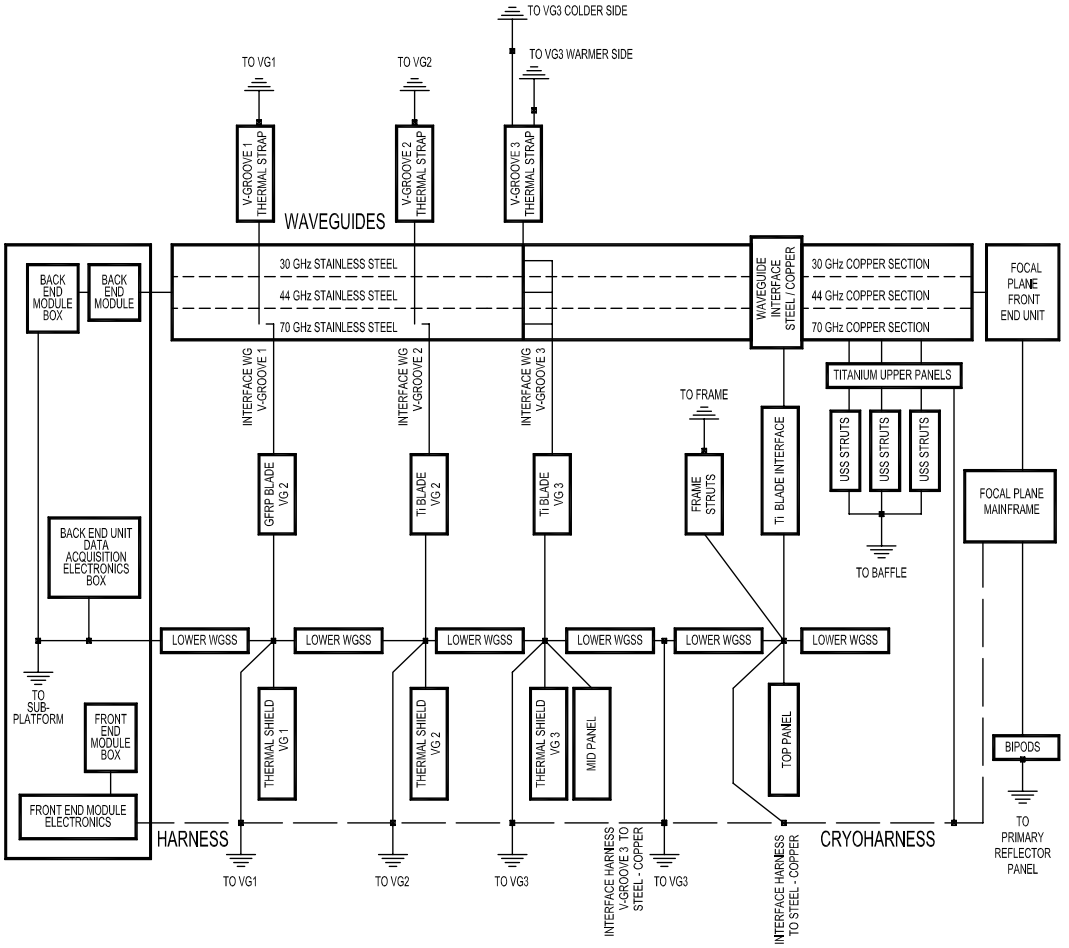

Fig. 9 Schematic of the Low Frequency Instrument, including the waveguide support structure (WGSS), upper support structure (USS), V-groove 1 (VG1), V-groove 2 (VG2), and V-groove 3 (VG3).

0.55 W, which is low enough to allow active cooling of the focal assembly to be performed. The radiometer array assembly carries the most critical elements of the LFI (the front-end unit and the waveguides) and of the HFI focal plane unit, with its 4 and 0.1 K cooler pipes. The radiometer array assembly interfaces thermally with the payload module structure, including the three V-grooves. A block diagram of the instrument is shown in Fig. 9 and an illustration is shown in Fig. 10.

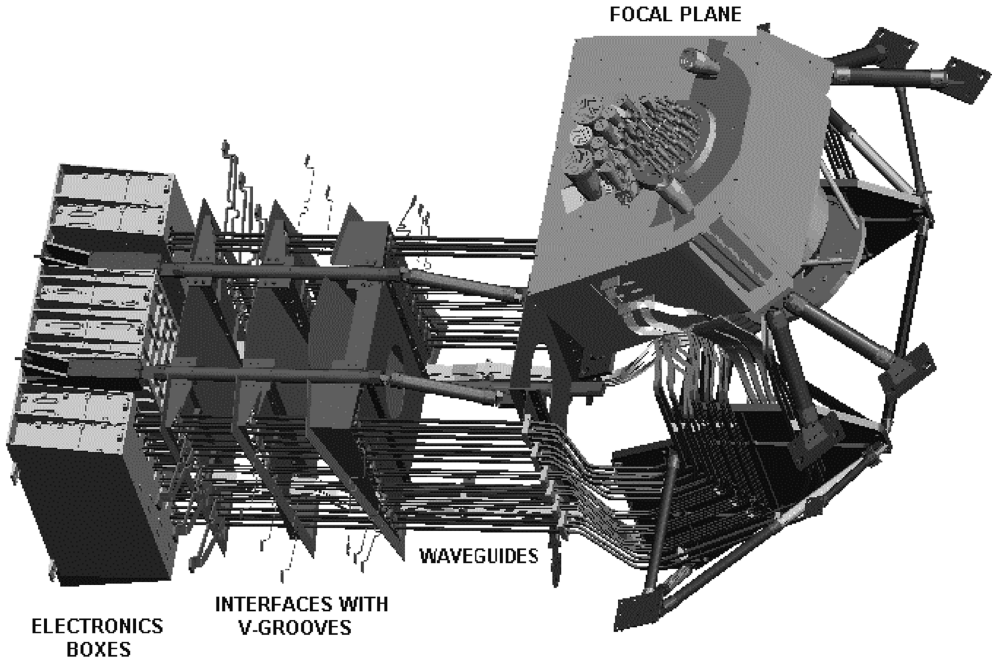

Fig. 10 View of the Low Frequency Instrument (shown integrated with the HFI focal plane unit).

The LFI reference load provides a stable blackbody signal at 4 K that is continuously compared against the CMB signal from the sky. The reference load consists of custom-shaped targets mounted on the HFI 4 K shield in front of LFI front-end modules. Each target contains an iron-loaded epoxy-absorbing material (Eccosorb CR110 and Eccosorb CR117), to achieve high emissivity at cryogenic temperatures. The thermal requirements are a radiative heat load onto the HFI of less than 1 mW and a thermal stability within the μK range.

2. High Frequency Instrument

The High Frequency Instrument is designed to produce high-sensitivity multifrequency measurements of the diffuse sky radiation in the frequency range of 100 to 857 GHz (wavelength range of 3.0 to 0.4 mm) [14]. The HFI makes use of an array of direct detection bolometric (thermal) detectors [15] that must be cryogenically cooled to achieve sufficient sensitivity and speed of response. The detectors must be cooled to 0.1 K and the feedhorns to below 5.5 K. In addition to the stringent requirements on temperature, the temperature stability must also be carefully controlled. The required temperature noise spectral density must be better than 20 nK $Hz^{-0.5}$ at 100 ± 5 mK, 28 μK $Hz^{-0.5}$ at a temperature lower than 2.1 K, and 10 μK $Hz^{-0.5}$ at a temperature lower than 4.8 K. A schematic of the instrument is shown in Fig. 11.

The HFI uses three stages of active cooling at 4, 1.6, and 0.1 K. The 4 K stage cooling is provided by the helium JT cryocooler described earlier, whereas the 1.6 and 0.1 K stage cooling is provided by the $^3He/^4He$ dilution refrigerator, also described earlier. For cooldown, a thermal switch connects the 4 K stage with the 18 K stage. This gas-gap switch functions by making use of temperature-dependent adsorption properties of hydrogen gas onto carbon; it remains fully closed when the 18 K stage temperature is above 64 K and is fully open when this temperature is below 52 K. A similar switch, using helium as the working fluid, connects the 4 K stage to the 1.6 K stage; it remains fully closed when the 18 K stage temperature is above 25 K and is fully open when this temperature is below 17 K [16].

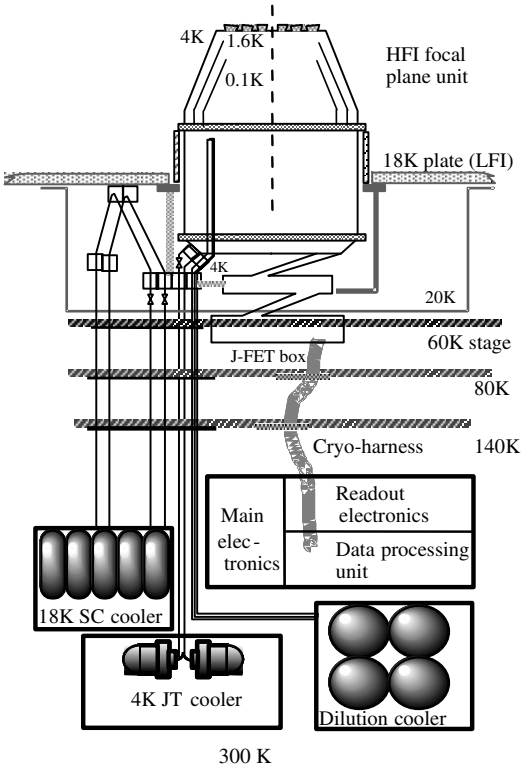

Fig. 11 Schematic of the High Frequency Instrument and sorption cooler system.

III. Thermal Performance Verification by Analysis

In addition to the overall objective of verifying the performance of Planck by analysis, the system-level thermal model has a number of specific goals: enable tradeoffs to be performed to optimize the thermal design; perform sensitivity analyses to assess the robustness of the design; perform sensitivity analyses to understand the degradation in performance over the course of the mission; provide information on the cooling margins available at each stage in the cooling chain; make predictions to guide the planning of the testing program; and allow quantification of temperature stability levels at each of the stages of the cooling chain. The temperature stability must also be evaluated for those components for which there is a line of sight to the detectors, because such temperature fluctuations would lead to additional noise on the detectors and need to be disentangled from the scientific signal.

The following sections describe the thermal design and modeling of each of the major subsystems of the spacecraft, followed by a description of the full system model. The subsystem models were significantly reduced in size and complexity to obtain a final system model that can run with a reasonable computational runtime. For the active coolers in particular, this means that phenomenological models were used to describe their thermal behavior in a simplified manner [17].

A. Subsystem Thermal Models

1. SVM

For the purposes of the system model, focused on PLM thermal study, the full detailed thermal SVM model of ~2500 thermal nodes was reduced to 115 nodes. Furthermore, all SVM nodes (except MLI outer layers) are boundary nodes.

2. PLM

The PLM thermal model (~1700 thermal nodes) includes complete modeling of the primary and secondary reflectors, baffle, V-grooves, structures, struts, all piping, and all harnesses. The performance of the V-groove radiator as predicted by the detailed PLM thermal model is shown in Fig. 12. The central sections of the three shields were predicted to achieve temperatures of 135–149, 95–100, and 48–53 K, respectively.

3. Hydrogen Sorption Cooler

Although a detailed thermal model was developed by NASA's Jet Propulsion Laboratory to guide the design of the cooler, a simplified thermal model is used here to calculate the heat loads of the hydrogen flow on each of the precooler stages and to calculate the final cooling power at the cold end. The heat load Q_{PC1} on the first (warmest) V-groove radiator is calculated according to

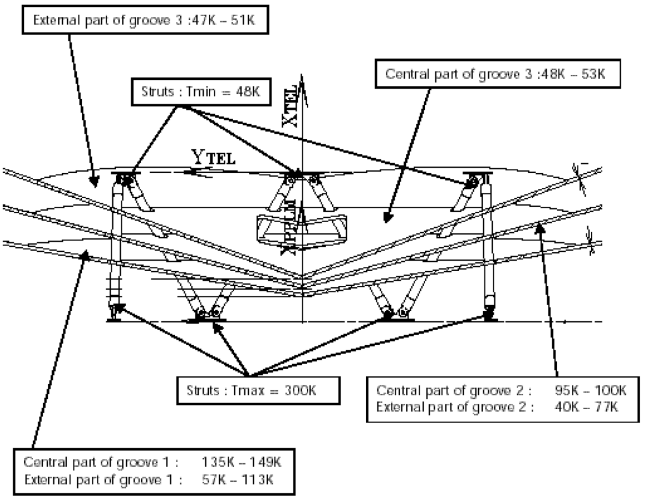

Fig. 12 Predicted temperatures of the V-grooves and struts.

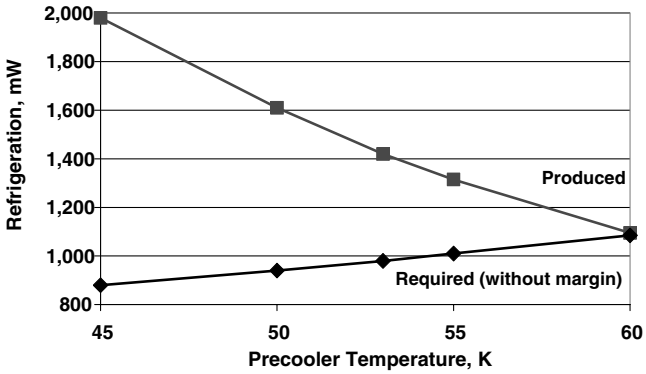

Fig. 13 Refrigeration produced and required (without margin) for the 20 K sorption cooler, as a function of the cooler's temperature at its coldest interface with the third V-groove radiator.

$$Q_{\mathrm{PC1}} = M \cdot \{[H(P_{\mathrm{HIGH}}, T_{\mathrm{SCC}}) - H(P_{\mathrm{HIGH}}, T_{\mathrm{PC1}})] - E_{01} \cdot [H(P_{\mathrm{LOW}}, T_{\mathrm{SCC}}) - H(P_{\mathrm{LOW}}, T_{\mathrm{PC1}})]\} \tag{1}$$

Similar equations apply for the heat load on the other precooler stages and for the heat lifted through the JT expansion at the coldest stage.

The refrigeration produced depends very sensitively on the precooling temperature of the third V-groove. Figure 13 shows how this refrigeration produced decreases with increasing precooler temperature at the interface with the V-groove radiator. The same figure also shows how the amount of refrigeration required increases with increasing precooler (third V-groove) temperature. It can be seen that there is little margin between available and required cooling power for the maximum allowable interface temperature of 60 K.

4. *Helium Joule–Thomson Cooler*

A detailed thermal model of the JT cooler was developed at the Rutherford Appleton Laboratory to predict the cooler performance. This model calculates the thermal loads at each precooler temperature stage and the final cooling power based on the cooler geometry, compressor temperatures and pressures, precooling stage temperatures, and helium mass flow rate. A simplified version of this thermal model was developed for use in the system thermal model, in which precooling loads from the helium fluid are modeled simply as a function of precooling stage temperatures and compressor temperature:

$$\text{thermal load on 20 K stage} = f\left\{\begin{array}{l}\text{compressor temperature}\\ \text{50 K precooling temperature}\\ \text{20 K precooling temperature}\end{array}\right\} \tag{2}$$

$$\text{thermal load on 20 K stage} = f\left\{\begin{array}{l}\text{50 K precooling temperature}\\ \text{20 K precooling temperature}\end{array}\right\} \tag{3}$$

Operational temperature ranges are identified for each cooling stage, and detailed algorithms are used to calculate a number of precooling load values over that range. Regression analysis is then used to derive parametric equations to fit the data. Figure 14 shows the predicted cooling power at a nominal cold head temperature of 4.5 K as a function of the temperature of the 20 K precooling stage and compared with the cooling requirement (with and without the assigned 30% margin). It can be seen that for a precooling temperature above 18.4 K, there is no excess cooling power, compared with the requirement (with margin). This analysis underlines the need to have a combination of adequate precooling and sufficiently low heat load at the interface of the HFI with the sorption cooler.

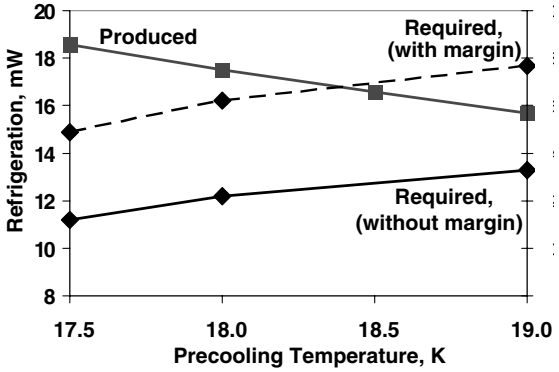

Fig. 14 Refrigeration produced and required for the 4 K Joule–Thomson cooler, as a function of its interface with the sorption cooler coldest stage.

5. *Helium Dilution Cooler*

The open-cycle dilution cooler operates at an excess of ^{3}He greater than the 6.4% solubility limit below 0.1 K, and the theoretical cooling power is therefore only a function of the ^{4}He mass flow and the temperature. At constant isotope mass flow, the temperature response of the cold tip is accurately described [18] by a classical square-temperature law below 0.4 K:

$$Q = \dot{n}_4 \cdot q_{\mathrm{DIL}} \cdot T^2 - Q_0 \tag{4}$$

where $\dot{n}_4$ is the mass flow rate of ^{4}He, q_{DIL} for the Planck dilution cooler is $\sim$3 J K^{-2} mol^{-1}, and Q_0 is an estimation of the losses due to viscous dissipation and due to thermal conduction in supports and wires. At unit-level testing, the Planck dilution cooler has achieved 0.1 K, with the required 100 nW of heat load applied [19]. However, this low level of cooling power creates difficulty for inclusion within a system thermal model that must simultaneously account for power levels of several tens of watts elsewhere in the system. It is therefore impractical to predict the performance of the dilution cooler at the system level. Instead, for cooldown analyses, the system thermal model uses parametric equations to apply temperature-dependent heat lifts at the 0.1 and 1.6 K stages. Once each stage reaches its nominal temperature, the thermal model sets the stage as a boundary node. The model also includes the thermal conduction along the pipes and harness, as well as the fluid loads on the third V-groove and on the HFI 18 K stage.

6. *Low Frequency Instrument*

The LFI thermal model has 106 thermal nodes, structured in three parts. The focal plane unit at 22.5 K comprises the main frame, the front-end unit, and the first liquid-vapor heat exchanger for the 20 K sorption cooler. At intermediate temperatures, the waveguides are modeled as one beam, accounting for the different materials and thermo-optical properties for the different stages. The waveguide support structure is modeled to include the thermal strap connections to the waveguides. Because of the large temperature range spanned by the electrical harness, this harness has detailed modeling. Finally, the warm electronics box (the back-end unit) at ambient temperature is modeled as a boundary node. The power dissipation of the electronic componentsi as condensed into three nodes. In the separate reference load thermal model, two reference load targets are represented per diffusion node, each coupled to the LFI 20 K stage by means of radiative conductors that take into account the target surface and the Eccosorb high infrared emissivity ($\varepsilon \approx 1$).

The predicted heat loads at each of the LFI stages are given in Table 3.

Table 3 Low Frequency Instrument heat load predictions and allocations

Interface	Predicted temperature, K	Predicted total heat load with margin, mW	Heat load allocation, mW
V-groove 1	166	463	710 for both instruments
V-groove 2	106	337	560 for both instruments
V-groove 3	51.4, 57.6	2939	5370 for both instruments

Table 4 High Frequency Instrument heat load predictions and allocations

Interface	Predicted temperature, K	Predicted total heat load with margin, mW	Heat load allocation, mW
V-groove 1	165	60	710 for both instruments
V-groove 2	110	24	560 for both instruments
V-groove 3	50	744	5370 for both instruments
20 K stage	18	149	190
4 K stage	5	11	15
1.6 K stage	1.6	0.3	0.4
0.1 K stage	0.1	−0.0001 (set to available cooling power)	0.0001

7. High Frequency Instrument

There are three versions of the HFI thermal model: a detailed version for steady-state analysis, a reduced version for transient analysis, and a coarse version for cooldown duration calculations. The models include the details of all HFI stages, down to 4 K. The warm power amplifier unit electronics box is modeled, as is the JFET box that contains the first stage of amplification of the detector signals and that is heat sunk to 50 K. The electrical harness is modeled to account for the heat loads it imposes on the V-grooves, the struts of the cryostructure, and the rear panel. The models were created using IDEAS-TMG, with which the main HFI thermal analyses were also performed, and then exported to ESATAN format for the purposes of inclusion in the system-level model. The calculated heat loads at each of the HFI stages are given in Table 4.

The steady-state model sets the 1.6 K stage as a boundary node and does not include details of the 0.1 K stage. The transient model does not include the 1.6 and 0.1 K stages, but cooldown calculations can be performed down to a temperature of 4 K, after which the model relies on experimental data from subsystem unit-level testing to account for the remaining time needed to cool down from 4 to 0.1 K.

B. System Thermal Model Description and Predictions for Flight

We now describe the content of the overall system-level model, together with factors influencing how it was built. We then describe the predictions derived from the model for the cooldown and steady-state performance of Planck.

1. Description

To calculate the radiative couplings between the various surfaces of the thermal nodes, a geometrical model describing the SVM, PLM, and the two payload instruments was built and processed by ESARAD. The large number of shells used for the detailed and system models is conveyed in Table 5. The resulting radiative couplings were assembled, together with the conductive couplings, the heat loads, and the thermal capacitances to build three system thermal models in ESATAN format. These models represent the following configurations: the flight model in space, the flight model in the test facility, and the cryogenic qualification model in the test facility. Nominal and hot case models for all configurations were created. Because of computational processing time constraints, a version of the system model was simplified further to enable transient cooldown cases to be analyzed.

A number of modeling issues needed to be addressed in how the system-level model was built, including configuration control, software compatibility, margin philosophy, model runtime, and allocation of node-number ranges. Rigorous configuration control was implemented to ensure that all model versions were clearly identified, all model updates were fully documented and distributed, and improvements at the subsystem-model level were reflected at the system level. Software compatibility was also a key issue that needed to be carefully addressed. Although, in most instances, the subsystem models were built using ESARAD/ESATAN software, in some cases, it was necessary to convert models that were originally created in other formats (for example, IDEAS-TMG). For this adaptation, conversion utilities were generally found to give acceptable results after correlation at the subsystem level. In addition, a generic margin philosophy was agreed upon at the outset of this program of work. To prevent excessively conservative models being generated, margins were not taken into account in subsystem models, but were included at the system level. With respect to runtime, the steady-state system model took under 1 h to run, and the cooldown system model took several hours to run. Node-numbering ranges were allocated to all subsystem models to facilitate integration into the system-level model.

2. Flight Predictions

The predicted interface temperatures at the end of the passive cooldown are presented in Table 6. It can be seen that all predictions

Table 5 Nodal breakdown of detailed subsystem and overall system models

Subsystem	Detailed models	Implementation in system model	
		Steady state	Transient
SVM	∼2500	115	39
V-grooves	666	666	171
Baffle	12	12	6
Mirrors, support frames, and struts	1000	1000	222
LFI	∼300	106	106
HFI	IDEAS-TMG model	257	82
Sorption cooler	Detailed SINDA model	34 nodes with simplified algorithms	
4 K Joule–Thomson cooler	Detailed algorithms	8 nodes with simplified algorithms	
Dilution cooler	Detailed algorithms	8 nodes with simplified algorithms	
Total		2206	676

Table 6 Predictions of system thermal model for flight configuration in orbit

Subsystem	Interface	Required maximum temperature, K	Maximum predicted temperature in-flight, K
LFI waveguides	VG1	170	165.4
	VG2	120	99.6
	VG3	60	55.0
Sorption cooler	VG1	170	155.9
	VG2	120	98.7
	VG3	60	53.7
	LFI focal plane	22.5	20.3
	HFI ring	19.0	18.5
HFI JFET box	Rear panel	60	54.5
4 K cooler	VG3	60	55.6
	4 K plate	5.2	4.8
Dilution cooler	VG3	60	55.6
	Detectors	0.1	0.1 (set point)
Primary reflector	N/A	50	46.4
Secondary reflector	N/A	50	48.3

for in-flight interface temperatures are compliant with the requirements, giving a good level of confidence in the design approach. In particular, the interface temperature of the sorption cooler with VG3 is significantly colder than 60 K.

The predicted temperatures for the coldest parts of the two instruments were also in agreement with the requirements. A series of sensitivity analyses were run to assess how the system would perform under non-nominal conditions. A number of cases were chosen based on areas of uncertainty, for example, increased cooler loads, increased power dissipation levels, and reduced heat rejection efficiency radiators. The studies showed that the model was robust and helped to identify critical areas of the system design.

Further design verification and model validation were then performed by actual testing in a cryogenic facility, guided by

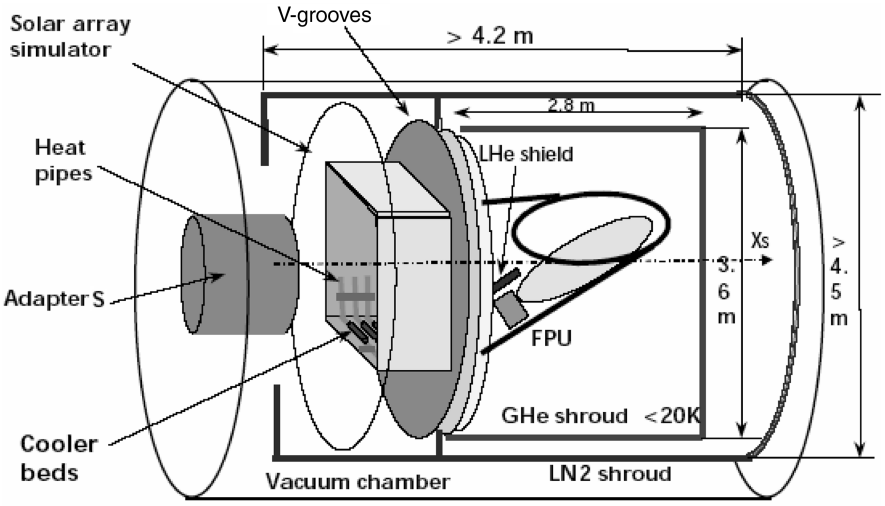

Fig. 15 Planck cryogenic test facility.

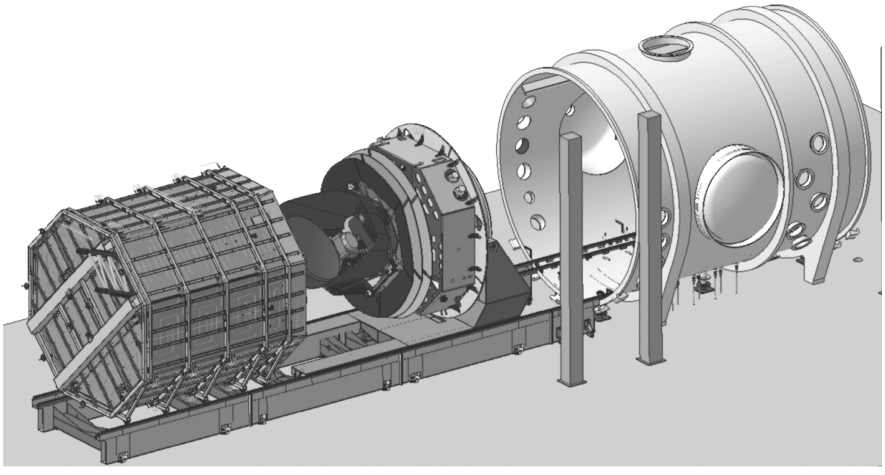

Fig. 16 Thermal tent, Planck spacecraft, and vacuum chamber before integration.

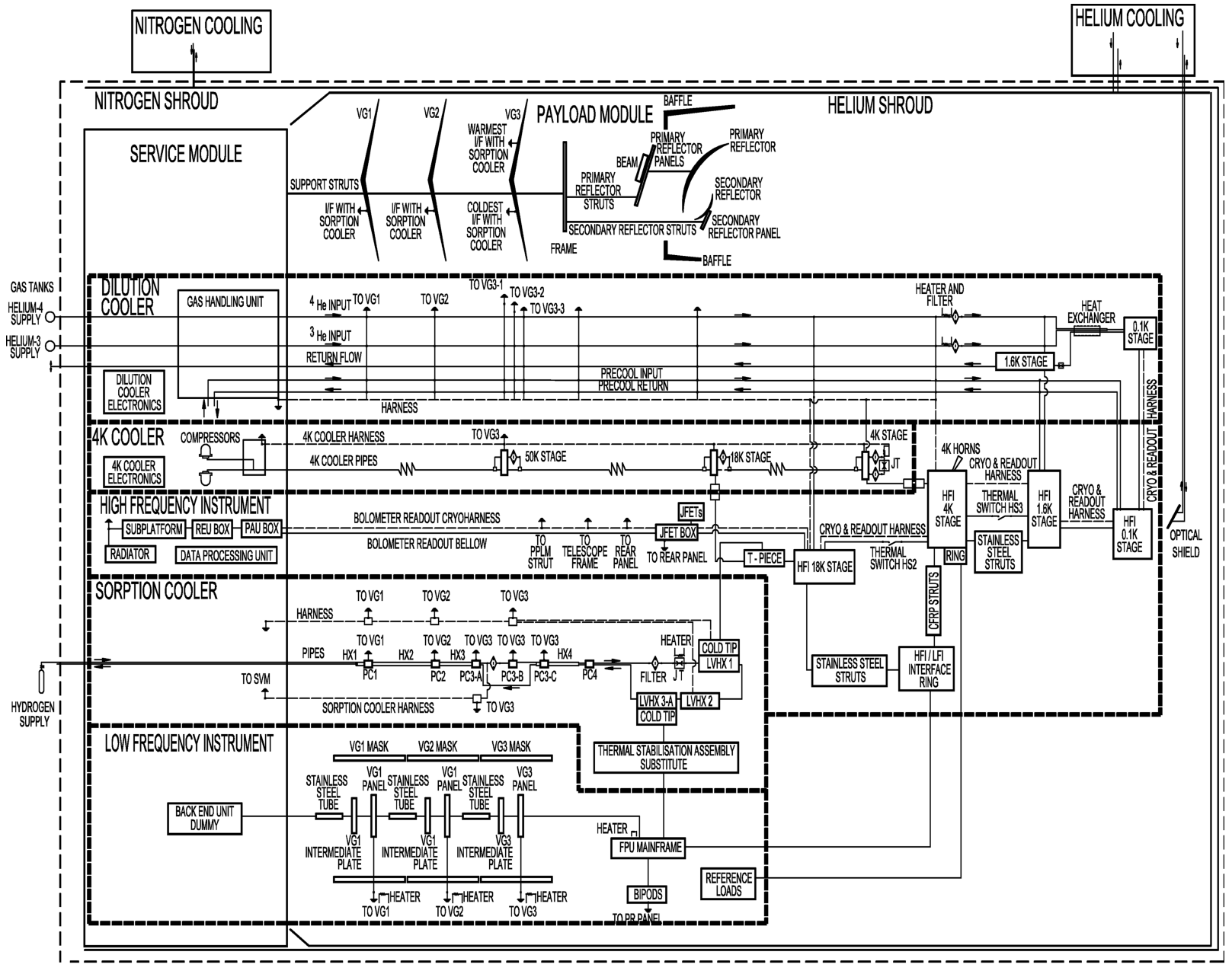

Fig. 17 Schematic of Planck thermal system model (cryogenic qualification model in test facility).

adaptation of the system-level thermal model in accordance with the configuration of the test specimen and the characteristics of the test facility.

IV. Thermal Performance Verification by Test

The Planck PLM was initially qualified by test at the cryogenic qualification model level. In preparation for this, the system thermal model was modified to reflect the test configuration and to include the test chamber and then used to generate test predictions and to anticipate potential problem areas (e.g., uncertainty in the shroud temperatures). In addition, another important task of the system model was to predict the duration of the cooldown to optimize the cooldown procedure. During the test, the temperatures on the PLM were acquired by 64 platinum resistance thermometers (Minco PT100 S651) and 46 silicon diodes (Lakeshore DT470), all with an accuracy of ± 12 mK at 77 K. Upon completion of the thermal test, the model was correlated to improve its applicability for making cooldown and steady-state predictions for the flight model performance. The detailed correlation will be presented elsewhere; here, we will focus on an initial summary of these data.

A. Test Specimen

The test specimen consisted of the cryogenic qualification model of the PLM, with a simplified substitute used for the SVM. Because of scheduling reasons, the qualification model of the LFI was not available for this CQM test sequence. It was therefore necessary to replace this with mass and thermal dummies of the focal plane unit, the waveguides, and the back-end unit. This structure imposed the allocated thermal loads on the passive radiator and provided the HFI focal plane with representative mechanical and thermal interfaces. Accordingly, the system thermal model includes an appropriately modified version of the LFI thermal model. Similarly, the compressors for the 20 K sorption cooler were unavailable for this test and were replaced by a supply of high-pressure hydrogen from gas bottles. The thermal interaction with the SVM radiator of the compressors was simulated using heaters. A precooling loop was used to expedite the cooldown of the coldest stages of the HFI, which are thermally isolated from the remainder of the instrument. The effect of this precooling loop was included in the thermal model cooldown calculations. The complete Planck spacecraft, including the full LFI and the 20 K cooler compressors, will be tested during the PFM test campaign.

B. Spacecraft Test Facility

The Planck spacecraft was tested at the system level at representative cryogenic temperatures in the test facility at the Centre Spatiale de Liège. The test setup is shown in Figs. 15 and 16. The large size of the spacecraft, the extreme temperature range of operation, the miniscule level of cooling power at the coldest temperature, and the demanding requirements on temperature and mechanical stability all led to a test that was extremely challenging to perform. The test chamber made use of shrouds cooled to ~ 10 K by cold gaseous helium and additional shrouds cooled to ~ 80 K by cold gaseous nitrogen, to cool down the spacecraft radiatively, as close as possible to flight configuration (i.e., with very highly absorptive shrouds and appropriate shielding). A 4 K Eccosorb optical shield filled with liquid helium and with a temperature stability of ± 1 mK over 60 s was placed in front of the focal planes, providing a cold reference source for the HFI detectors. Baffles were used to reduce stray light reflections off the shrouds from the warm SVM to the cold PLM. Because the performance of the Planck cryogenic cooling chain depends very sensitively on the integrity of the vacuum level in the test chamber, a large charcoal panel cooled to 4 K was used as a getter to cryopump any residual helium gas from the test volume that might originate either from the test facility or from the warm parts of the coolers located on the SVM.

C. CQM System Model Predictions

An overall schematic of the system model, shown in Fig. 17, gives an appreciation of the complexity of the interactions between the different subsystems on Planck. This version of the thermal model includes the nitrogen and helium shrouds and the optical shield at 4 K in front of the payload instrument detectors. In this figure, HS is the heat switch, REU is the readout electronics unit, JFET is the junction field-effect transistor, PAU is the power amplifier unit, LVHX is the liquid-vapor heat exchanger, PC is the precooler, CFRP is the carbon-fiber-reinforced polymer, and JT is the Joule–Thomson expander.

The system-level thermal model was used to calculate the expected cooldown time, which was important 1) to optimize the switch-on sequences for the different elements of the active cooling chain and 2) to facilitate the planning of the complex test sequence. The predicted cooldown for 12 days following the start of cooling is presented in Fig. 18, which shows that passive cooldown to 60 K is predicted to take between 2.6 to 4.4 days. The colder V-grooves take longer to cool down, due to their increasing levels of thermal isolation from the rest of the warmer environment.

The predicted cooldown from 12 to 20 days is shown in Fig. 19. The HFI precooling loop is switched on after 15 days, the 4 K cooler after 16 days, and the dilution cooler after 17 days. The 4 K plate is expected to achieve its base temperature after 18 days.

The predicted steady-state temperatures are given in Table 7, which also lists the required temperatures at the relevant interfaces.

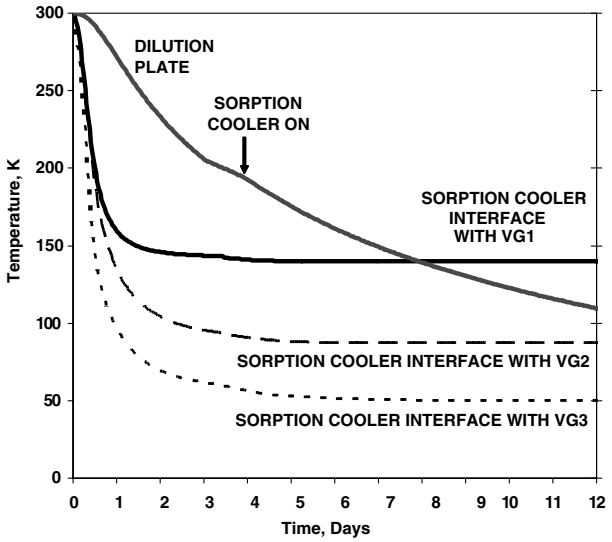

Fig. 18 Predicted CQM cooldown performance (0–12 days).

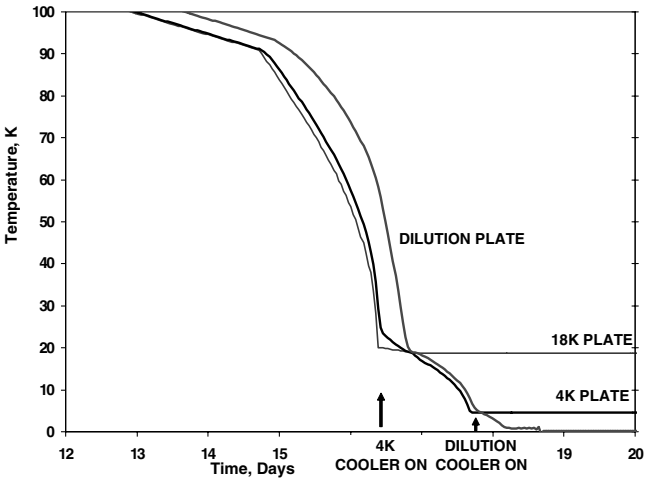

Fig. 19 Predicted CQM cooldown performance (12–20 days).

Table 7 Predicted temperatures for CQM test

Subsystem	Interface	Required maximum temperature, K	Predicted CQM test temperature, K	
			Min	Max
LFI waveguides	VG1	170	150.8	167.8
	VG2	120	83.5	93.9
	VG3	60	48.4	56.6
Sorption cooler	VG1	170	134.6	146.0
	VG2	120	84.8	94.5
	VG3	60	46.9	54.8
	LFI focal plane	22	20	20
HFI JFET box	Rear panel	60	45.9	52.8
4 K cooler	VG3	60	48.4	56.6
	4 K plate	5.2	4.8	4.8
Dilution cooler	VG3	60	46.7	54.5
	Detectors	0.1	0.1 (set point)	0.1 (set point)
Primary reflector	N/A	50	42.0	47.9
Secondary reflector	N/A	50	43.1	49.9

In every case, the predicted CQM test temperature is lower than the required maximum temperature, giving confidence in the design of the CQM hardware and the test facility.

D. CQM Test Performance

The cooldown of the CQM cryogenic chain during test is shown in Fig. 20. Passive cooldown to below 60 K was achieved in 3.5 days, which was within the prediction from the thermal model (minimum 2.6 days, maximum 4.4 days). After 12 days, the steady-state temperatures of the sorption cooler interfaces with the three V-groove radiators had stabilized to 148, 93, and 48 K. This compared favorably with the predicted temperatures after the first 12 days of 140, 87, and 50 K, respectively. The dilution cooler plate after this time was at 105 K, compared with the predicted value of 110 K.

As shown in Fig. 21, the cooldown of the HFI 4 K plate to 4 K took 18 days from the start of testing. This was in line with the prediction shown in Fig. 19. In general, the 0.1 K dilution and the 4 and 18 K plates cooled down more quickly than predicted, reaching 20 K approximately one day earlier than predicted. The final stages of cooldown were complicated by the presence of a cryogenic leak of helium, possibly from the test facility, but the 0.1 K cooler did reach its final required temperature, which enabled useful testing of the HFI focal plane detectors to be performed.

For steady state, the temperatures achieved at relevant interfaces with the passive cooling chain, compared with the minimum and maximum predicted temperatures, are shown in Table 8. It can be seen that all passive element temperatures achieved were lower than the maximum allowable levels for flight, with some telescope areas being even colder than predicted. The sorption cooler cold end functioned as required, albeit with fluid supply inputs not from thermal compressors but from hydrogen gas bottles that made it easier to achieve the required temperatures. The 4 K cooler operating temperature was a little higher than predicted, but nonetheless still cold enough and with enough cooling power to allow the dilution cooler to function correctly.

It can be concluded that the system thermal model provided an accurate prediction of the passive and active cooldown processes and that the overall verification and test program was therefore deemed to be successful. Further thermal model correlation is needed to evaluate the levels of temperature stability at different stages in the cooling chain. It should also be noted that although the on-ground tests conducted so far were successful, the thermal performance of the active cooling chain in a zero-gravity environment remains to be fully verified.

V. Thermal Modeling Lessons Learned

Several lessons were learned during the development of the system model. When constructing the model, it was necessary to make a tradeoff between size, required analysis accuracy, and runtime. The very challenging thermal requirements on Planck also meant that calculation of the temperature and heat flux for the colder areas of the instruments, for which requirements were the strictest, were at the limit of the software resolution. In addition, it was difficult to take into account all parasitic heat loads that can have a significant impact on the performance of the cryogenic cooling chain. Parasitic heat loads arising, for example, from gas conduction through outgassing or leaks could significantly modify the duration of the cooldown. Also, analyses were needed to assess whether certain thermal results represented real thermodynamic phenomena or were

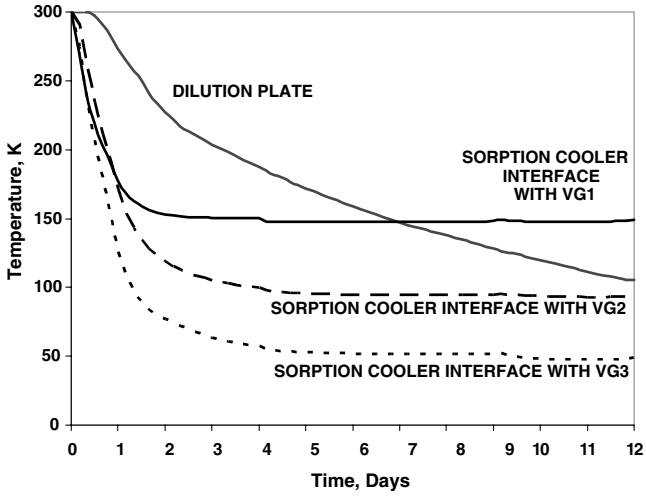

Fig. 20 Actual cooldown performance during CQM test (0–12 days).

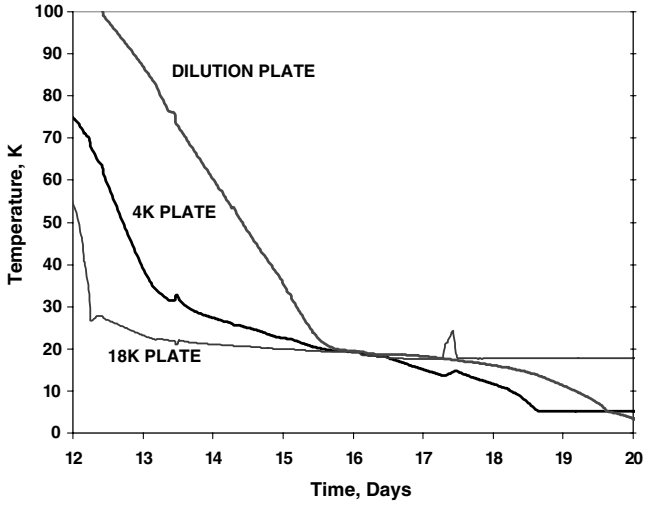

Fig. 21 Actual cooldown performance during CQM test (12–20 days).

Table 8 Comparison between predicted and achieved temperatures for CQM test

Subsystem	Interface	Required maximum temperature, K	Predicted CQM test temperature, K		Actual CQM test temperature, K	Deviation of actual temperature from predicted range, K
			Min	Max		
LFI waveguides	VG1	170	150.8	167.8	159.2	None
	VG2	120	83.5	93.9	94.3	+0.4
	VG3	60	48.4	56.6	49.8	None
Sorption cooler	VG1	170	134.6	146.0	148.4	+2.4
	VG2	120	84.8	94.5	93.2	None
	VG3	60	46.9	54.8	48.1	None
	LFI FPU	22.5	20	20	20	None
HFI JFET box	Rear panel	60	45.9	52.8	44.0	−1.9
4 K cooler	VG3	60	48.4	56.6	49.8	None
	4 K plate	5.2	4.8	4.8	5.3	+0.5
Dilution cooler	VG3	60	46.7	54.5	48.3	None
	Detectors	0.1	0.1 (set point)	0.1 (set point)	0.1	None
Primary reflector	N/A	50	42.0	47.9	40.7	−1.3
Secondary reflector	N/A	50	43.1	49.9	42.2	−0.9

instead numerical artifacts arising from the solution algorithms. The issue of improving model clarity and configuration control without unduly increasing runtime was also important, and this tradeoff must be performed with models of this level of complexity. The benefits of strict configuration control were made clear with the regular update and exchange of the subsystem models.

Because of the intricacy of the steady-state model and the capability of the software, it was necessary to perform tradeoffs and to define a minimum cutoff point, below which radiative links would not be output from the ESARAD software. The cutoff point, as defined by the software, merely discarded links below a specified value. At the same time, it was not possible to apply any weighting criteria according to the thermal mass of the components or according to their sensitivity to thermal fluctuations. This inability sometimes caused problems when analyzing the level of radiative heat loads on the cold instruments. When modeling thermally critical components, which are often found on the cold instruments, the components are typically discretized with a fine mesh of nodes, meaning that each individual node has a small surface area. Radiative links to these critical nodes are dependent on area and so are also typically small and likely to be below the software's minimum threshold. Thus, the total calculated radiative load onto a component made up of many small nodes could have been smaller than expected. Critical areas of the system model were examined in detail to ensure that this did not affect the model outputs. Subsequent to the creation of the system thermal model, newer versions of the ESATAN software were released that use more efficient computation algorithms, thus allowing much larger models to be built and thereby removing the need for a cutoff point.

VI. Conclusions

The design and cooling requirements have been presented for the cooling chain and focal plane instruments of the Planck spacecraft. The number and complexity of interactions between the different subsystems have led to the need to build a system-level thermal model of the complete spacecraft to assist in the performance verification program. As inputs into the system-level model, the detailed subsystem thermal models were simplified in a manner that captures important elements of the thermal behavior, while allowing for integration into a model system that has a manageable number of thermal nodes. Predictions for the thermal behavior of the flight model of Planck have given confidence in the in-orbit cryogenic performance. To complement the verification by analysis, verification by test was also performed and the initial test results were presented for the performance of the cryogenic qualification model of the spacecraft in the test facility. The cryogenic cooling chain reached its required base temperature of 0.1 K. The test results were compliant with the requirements and with the predictions from the system-level thermal model. Detailed correlation of these results is underway, including analysis of transient behavior and instrument thermal stability. A number of lessons learned from this modeling activity were described.

Acknowledgments

The full list of contributors to the research presented here is as follows: Ravinder S. Bhatia, Claudio Damasio, Bernard Guillaume, Astrid Heske, Christopher I. Jewell, Javier Martí-Canales, and Giuseppe Sarri [ESA, European Space Research and Technology Centre (ESTEC)]; Giorgio Baldan, Luca Pagan, Marco de Paoli, and Roberto Ferretti (Alcatel Alenia Space); Pradeep Bhandari and Christopher G. Paine (Jet Propulsion Laboratory, California Institute of Technology); Thomas W. Bradshaw, Martin R. Crook, Jayne Fereday, and Anna H. Orlowska (Rutherford Appleton Laboratory); Philippe Camus [Centre de Recherches sur les Très Basses Températures, Centre National de la Recherche Scientifique (CNRS)]; Benoît Demolder, Marie-Pierre Estienne, Emmanuel Gavila, and Jean-Bernard Riti (Alcatel Alenia Space); Jean-Jacques Fourmond and Fredrik Lejdstrom (Institut d'Astrophysique Spatiale, Université Paris-Sud/CNRS); Pierre Jamotton and Tanguy Thibert (Centre Spatial de Liège); and Luca Terenzi (Instituto Nazionale di AstroFisica, Istituto di Astrofisica Spaziale e Fisica Cosmica Bologna). We thank the teams involved in the design, assembly, integration, and testing of Planck.

References

[1] Hawarden, T. G., Crane, R., Thronson, H. A., Jr., Penny, A. J., Orlowska, A. H., and Bradshaw, T. W., "Radiative and Hybrid Cooling of Infrared Space Telescopes," *Space Science Reviews*, Vol. 74, Nos. 1–2, Oct. 1995, pp. 45–56.

[2] Gardini, B., Graf, G., and Ratier, G., "The Instruments on Envisat," *Acta Astronautica*, Vol. 37, No. 2, 1995, pp. 301–311.

[3] Riti, J.-B., Dubruel, D., Nadarassin, M., and Martin, P. P., "Planck Payload Module Design and Performance," *IR Space Telescopes and Instruments*, Vol. 4850, International Society for Optical Engineering, Bellingham, WA, 2003, pp. 749–763.

[4] Delouard, P., Krähenbühl, U., and Peikert, G., "Materials Characterisation at Cryogenic Temperatures for the Planck Telescope," *European Conference on Spacecraft Structures, Materials and Mechanical Testing* [CD-ROM], SP-581, European Space Agency Special Publication, Aug. 2005.

[5] Bard, S., "Advanced Passive Radiator for Spaceborne Cryogenic Cooling," *Journal of Spacecraft and Rockets*, Vol. 21, No. 2, 1984, pp. 150–155.

[6] Bard, S., "Development of a High-performance Cryogenic Radiator with V-groove Radiation Shields," *Journal of Spacecraft and Rockets*, Vol. 24, No. 3, 1987, pp. 193–197.

[7] Bhandari, P., Prina, M., Bowman, R. C., Jr., Paine, C., Pearson, D., and Nash, A., "Sorption Coolers Using a Continuous Cycle to Produce 20 K for the Planck Flight Mission", *Cryogenics*, Vol. 44, 2004, pp. 395–401.

[8] Prina, M., Bhandari, P., Bowman, R. C., Jr., Paine, C. G., and Wade, L. A., "Development of Gas Gap Heat Switch Actuator for the Planck

Sorption Cooler," *Advances in Cryogenic Engineering*, edited by Q.-S. Shu, Vol. 45, Kluwer Academic/Plenum, New York, 2000, pp. 553–560.

[9] Paine, C. G., "Characterization of Porous Sinter Materials as Joule–Thomson Restrictors for the Planck Sorption Cooler," *Cryogenics*, Vol. 44, Nos. 6–8, June–Aug. 2004, pp. 425–429.

[10] Bradshaw, T. W., and Orlowska, A. H., "Mechanical Cooling Systems for use in Space," *Journal of Aerospace Engineering*, Vol. 207, No. G1, 1993, pp. 21–25.

[11] Edwards, D. O., Efft, E. M., and Sarwinski, R., "Number Density and Phase Diagram of Dilute 3He-4He Mixtures at Low Temperatures," *Physical Review*, Vol. 177, 1969, pp. 380–391.

[12] Benoît, A., and Pujol, S., "Dilution Refrigerator for Space Applications with a Cryocooler," *Cryogenics*, Vol. 34, No. 5, May 1994, pp. 421–423.

[13] Mandolesi, N., Morgante, G., and Villa, F., "Low Frequency Instrument of Planck," *IR Space Telescopes and Instruments*, Vol. 4850, International Society for Optical Engineering, Bellingham, WA, 2003, pp. 722–729.

[14] Lamarre, J.-M., Puget, J. L., Piat, M., Ade, P. A. R., Lange, A. E., Benoit, A., De Bernardis, P., Bouchet, F. R., Bock, J. J., Desert, F. X., Emery, R. J., Giard, M., Maffei, B., Murphy, J. A., Torre, J.-P., Bhatia, R., Sudiwala, R. V., and Yourchenko, V., "Planck High Frequency Instrument," *IR Space Telescopes and Instruments*, Vol. 4850, International Society for Optical Engineering, Bellingham, WA, 2003, pp. 730–739.

[15] Yun, M., Beeman, J. W., Bhatia, R., and Bock, J. J., "Bolometric Detectors for the Planck Surveyor," *Millimeter and Submillimeter Detectors for Astronomy*, Vol. 4855, International Society for Optical Engineering, Bellingham, WA, 2003, pp. 136–147.

[16] Duband, L., "A Thermal Switch for Use at Liquid Helium Temperature in Space-borne Cryogenic Systems," *Proceedings of the 8th International Cryocooler Conference*, edited by R. G. Ross, Jr., 1st ed., Plenum, New York, 1995, pp. 731–741.

[17] Fereday, J., Bradshaw, T., Crook, M., Orlowska, A., Bhatia, R., Linder, M., Pin, O., Scommegna, A., and Vey, S., "Cryocooler Modelling Methodology," *Cryogenics*, Vol. 46, Nos. 2–3, 2006, pp. 183–190.

[18] Benoit, A., Camus, P., Crespi, P., Fourmond, J-J., Guyot, G., Madet, K., Sentis, L., and Triqueneaux, S., "Design of the Planck/HFI Dilution System," *Proceedings of the 19th International Cryogenic Engineering Conference (ICEC 19)*, Narosa, New Delhi, India, 2002, pp. 503–506.

[19] Sentis, L., Delmas, J., Camus, P., Guyot, G., and Blanc, Y., "Cryogenic Tests of a 0.1 K Dilution Cooler for Planck-HFI," *Proceedings of the 13th International Cryocooler Conference*, edited by R. G. Ross, Jr., 1st ed., Plenum, New York, 2005, pp. 533–542.

[20] Wade, L. A., Bhandari, P., Bowman, R. C., Jr., Paine, C., Morgante, G., Lindensmith, C. A., Crumb, D., Prina, M., Sugimura, R., and Rapp, D., "Hydrogen Sorption Cryocoolers for the Planck Mission," *Advances in Cryogenic Engineering*, edited by Q.-S. Shu, Vol. 45, Kluwer Academic/Plenum, New York, 2000, pp. 499–506.

I. Boyd
Associate Editor